CDF note 10855

Measurement of W Boson Polarization Fractions in Top Quark Decay to Lepton+Jets Events using a Matrix Element Analysis Technique with 8.7 fb^{-1} of Data

The CDF Collaboration
URL http://www-cdf.fnal.gov
(Dated: June 4, 2012)

We present measurements of the polarization of W bosons from top-quark t decays in the lepton plus jets channel $t\bar{t} \to W^+bW^-\bar{b} \to \ell\nu bq\bar{q}'\bar{b}$. Using 8.7 fb^{-1} of $p\bar{p}$ collisions in the full Run II data collected by the CDF II detector three measurements are performed. A simultaneous measurement of the fraction of longitudinal (f_0) and right-handed (f_+) W bosons yields the model-independent results $f_0 = 0.726 \pm 0.066(\text{stat}) \pm 0.067(\text{syst})$ and $f_+ = -0.045 \pm 0.043(\text{stat}) \pm 0.058(\text{syst})$ with a correlation coefficient of -0.51. A measurement of f_0 (f_+) constraining f_+ (f_0) to its standard model value of 0.0 (0.7) yields $f_0 = 0.686 \pm 0.042(\text{stat}) \pm 0.040(\text{syst})$ ($f_+ = -0.025 \pm 0.024(\text{stat}) \pm 0.040(\text{syst})$). The measurements correspond to a top-quark mass assumption of 172.5 GeV/c^2. All these results are consistent with standard model expectations.

Preliminary Results for 2012 Conferences

I. INTRODUCTION

Measurement of the polarization of the W boson from top-quark decay provides a clean probe for testing the $V-A$ structure of the weak interaction in the standard model (SM). Due to its large mass, in the SM the top quark decays before forming a bound state via the charged current weak interaction into a W^+ boson and a b quark [1], with a branching fraction above 99% [2]. In the SM at tree level [3], the W^+ boson is expected to have longitudinal polarization $f_0 = 0.696$, left-handed polarization $f_- = 0.303$, and right-handed polarization $f_+ = 3.8 \times 10^{-4}$ for a top-quark mass $m_t = 172.5$ GeV/c^2, a W-boson mass $M_W = 80.413$ GeV/c^2 [4], and a b-quark mass $m_b = 4.79$ GeV/c^2 [2]. In the limit of $m_b \to 0$, $f_0 = m_t^2/(2m_W^2 + m_t^2)$ and $f_+ = 0$. The uncertainties on the values of m_t, M_W and m_b [2] change the predictions at less than 1% (relative) level. The higher-order QCD and electroweak radiative corrections modify these predictions at the 1-2% (relative) level [5]. In beyond-the-SM scenarios the presence of anomalous couplings [3] in the tWb vertex can significantly modify the SM expectations. Measurements of W-boson polarization can be used to set constraints on the anomalous coupling vector and tensor form factors. At present the most precise experimental knowledge of the W-boson polarization comes from the Tevatron average [6] of the measurements in [7–9], and LHC [10].

II. OVERVIEW

This note presents an update of measurements of polarization of the W boson from top-quark decay [7]. The measurements of the W-boson polarization are performed for three different hypotheses of top-quark decay: (1) model-independent with simultaneous measurement of f_0 and f_+; (2) anomalous tensor couplings with measurement of f_0 for fixed f_+=0; and (3) anomalous right-handed couplings with measurement of f_+ for fixed $f_0 = 0.70$. In the current analysis we are using approximately three times larger data sample compared to that in [7]. In addition the current analysis is done based on a nominal top-quark mass of $m_t = 172.5$ GeV/c^2, where as the previous result was based on $m_t = 175$ GeV/c^2. The current assumption of m_t is closer to the World Average (WA) top-quark mass [2]. The top-quark mass assumption is used for the calibration, validation by performing simulated-experiments, evaluation of the relevant systematic uncertainties and obtaining the result from the data. We provide a dependence of the measured polarization fractions on the top-quark mass. However it is important to perform the measurement at or very close to the WA top-quark mass in order to provide a better estimation of the systematic uncertainties; this is more important in this analysis due to the expected improvement in statistical precision.

III. DATASET

The measurement is based on a data set with an integrated luminosity of 8.7 fb^{-1} acquired by the Collider Detector at Fermilab (CDF II) [11] from $p\overline{p}$ collisions at $\sqrt{s} = 1.96$ TeV. The data used are collected using high-transverse-momentum (p_T) [12] central (pseudorapidity [12] $|\eta| < 1.1$) electron and muon triggers and a trigger that requires large missing transverse energy $\not\!\!E_T$ [12] with either an energetic electromagnetic cluster or two separated jets ($\not\!\!E_T$+jets) [13]. The $\not\!\!E_T$+jets trigger is used to select additional events with high-p_T muons, which are not selected by the lepton triggers.

IV. METHOD

We use a data sample enriched in $t\overline{t} \to W^+bW^-\bar{b} \to \ell\nu bq\bar{q}'\bar{b}$ events, where one of the W bosons decays hadronically and the other leptonically. We assume that the $t\overline{t}$ production mechanism is in agreement with the SM. The polarization fractions are obtained by applying a likelihood technique based on the theoretical matrix elements for both the dominant signal process, $q\bar{q} \to t\overline{t}$, and the main background process, inclusive production of W+jets. This method uses the kinematic and topological information from the event and integrates over poorly known parton-level quantities. This technique was first developed for the measurements of top-quark mass and f_0 constraining f_+ to its SM value [14], and has been further developed for the measurements in [7]. The matrix element is expressed in terms of the W-boson polarization fractions and the cosine of the angle θ^* between the momentum of the charged lepton or down-type quark in the W-boson rest frame and the momentum of the W boson in the top-quark rest frame. Therefore we extract information on the W-boson polarization from both the leptonic and hadronic W-boson decays. Previous CDF measurements using different techniques[15, 16] used only information from the leptonic decay. While the information from the hadronic W-boson decay carries a sign ambiguity in $\cos\theta^*$ since we are unable to identify the down-type quark jet, its inclusion still improves the sensitivity to the f_0 polarization fraction. The analysis in described in [7]

and in this note improves the statistical sensitivity on f_0 by 20% relative to the best previous CDF measurement [15] for the same event sample. The latest D0 measurement also utilizes information from both the leptonic and hadronic W-boson decays [9].

The polarization fractions are determined using an unbinned likelihood function L maximized with respect to f_0, f_+, and the fraction of events consistent with the $t\bar{t}$ signal hypothesis, C_s,

$$L(f_0, f_+, C_s) = \prod_{i=1}^{N} [C_s \frac{P_s(x; f_0, f_+)}{\langle A_s(x; f_0, f_+)\rangle} + (1 - C_s)\frac{P_b(x)}{\langle A_b(x)\rangle}].$$

Here N is the number of observed events, x is a set of observed variables, and $\langle A_s\rangle$ and $\langle A_b\rangle$ refer to the average acceptances for $t\bar{t}$ and W+jets background events, respectively. The dependence of the $t\bar{t}$ signal acceptance on the polarization fractions is accounted for in $\langle A_s\rangle$. The signal probability P_s and background probability P_b densities are constructed as in [17] by integrating over the appropriate parton-level differential cross section convolved with the proton parton distribution functions (PDFs). The parton four momenta are estimated from the single lepton and the four highest transverse energy E_T [12] jets in the event, and transfer functions derived from Monte Carlo (MC) are used to unfold the detector resolution effects. There is an ambiguity in the jet-parton assignments and all permutations are used for each event.

The signal differential cross section uses the leading-order matrix element of the $q\bar{q} \to t\bar{t}$ process [18], expressed in terms of $\cos\theta^*$ and the polarization fractions:

$$|M|^2 = \frac{g_s^4}{9} F_\ell \bar{F}_h (2 - \beta^2 \sin^2\theta_{qt}),$$

where g_s is the strong coupling constant, θ_{qt} describes the angle between the incoming parton and the top quark in the rest frame of the incoming partons, and β is the velocity of the top quarks in the same rest frame. The factors F_ℓ and $\bar{F}_h$ correspond to the top quarks with a leptonic and a hadronic W-boson decay, such that:

$$\begin{aligned} F_\ell = \frac{2\pi g_W^4 m_{\bar{\ell}\nu}^2}{3 m_t \Gamma_t} (2E_b^{*2} + 3E_b^* m_{\bar{\ell}\nu} + m_b^2)(\frac{3}{8}(1 + \cos\theta^*)^2 f_+ \\ + \frac{3}{4}(1 - \cos^2\theta^*) f_0 + \frac{3}{8}(1 - \cos\theta^*)^2 (1 - f_0 - f_+)). \end{aligned}$$

Here g_W is the weak coupling constant, $m_{\bar{\ell}\nu}$ is the invariant mass of the lepton and neutrino, Γ_t is the width of the top quark, m_t and m_b are the masses of the top quark and b quark, respectively, and $E_b^* = \frac{m_t^2 - m_b^2 - m_{\bar{\ell}\nu}^2}{2 m_{\bar{\ell}\nu}}$. The hadronic factor $\bar{F}_h$ is similar, with the exception that we do not distinguish between up-type and down-type quarks from W-boson decay and use the average $\bar{F}_h$ related to the two permutations. The background differential cross section uses the sum of matrix elements for W+jets from the VECBOS [19] MC generator.

V. EVENT SELECTION

Candidate events for the lepton plus jets final state are selected to have a single, isolated electron or muon candidate with $E_T > 20$ GeV, large $\not\!\!E_T$ in the event ($\not\!\!E_T > 20$ GeV) as expected from the undetectable neutrino, and at least four jets with $E_T > 20$ GeV. Jets are reconstructed using a cone algorithm with radius $\Delta R = 0.4$ in $\eta - \phi$ space, and their energies are corrected for non-uniformities in the calorimeter response as a function of jet η, multiple $p\bar{p}$ interactions, and the hadronic jet energy scale of the calorimeter [20]. Of these jets, we require at least one to have originated from a b quark by using an algorithm that identifies a long-lived b hadron through the presence of a displaced vertex (b tag) [21]. Backgrounds to the $t\bar{t}$ signal arise from multi-jet QCD production (QCD), W-boson production in association with jets (W+jets), and electroweak backgrounds (EWK) composed of diboson (WW, WZ, ZZ) and single top-quark production. The W+jets background includes b-flavored jets as well as light-flavored jets (including charm-flavored jet) incorrectly identified as b jets.

A detailed description of the background estimation can be found in Ref. [22]. Table I shows the expected sample composition assuming a $t\bar{t}$ cross section of 7.4 pb. There are overlapping events between those collected by the high-p_T lepton triggers and the $\not\!\!E_T$+jets trigger which are included in the central e and μ categories, and are eliminated from $\not\!\!E_T$+jets category.

TABLE I: Number of expected and observed events in 8.7 fb^{-1} assuming a $t\bar{t}$ cross section of 7.4 pb.

Process	Central e	Central μ	$\not\!\!E_T$+jets μ
$t\bar{t}$	923 ± 93	696 ± 54	441 ± 44
W+jets	160 ± 41	125 ± 19	106 ± 21
EWK	36 ± 17	27 ± 11	16 ± 8
QCD	121 ± 48	6 ± 2	7 ± 3
Total Expected	1239 ± 113	853 ± 59	569 ± 50
Observed	1226	804	544

The HERWIG [23] MC generator is used to model the $t\bar{t}$ signal events with $m_t = 172.5$ GeV/c^2. For estimation of various systematic uncertainties and background modeling MC samples are created using the PYTHIA [24] generator, and ALPGEN [25] or MADEVENT [26] or MC@NLO [27] with PYTHIA or HERWIG supplying the parton shower and fragmentation. The QCD background is modeled using data control samples. The signal and background modeling has been extensively checked. Figure 1 compares the observed data and the MC-predicted distributions of different kinematic variables. We have validated the background model by studying a high-statistics control sample of W+jets candidates extracted by vetoing events containing b-tagged jets.

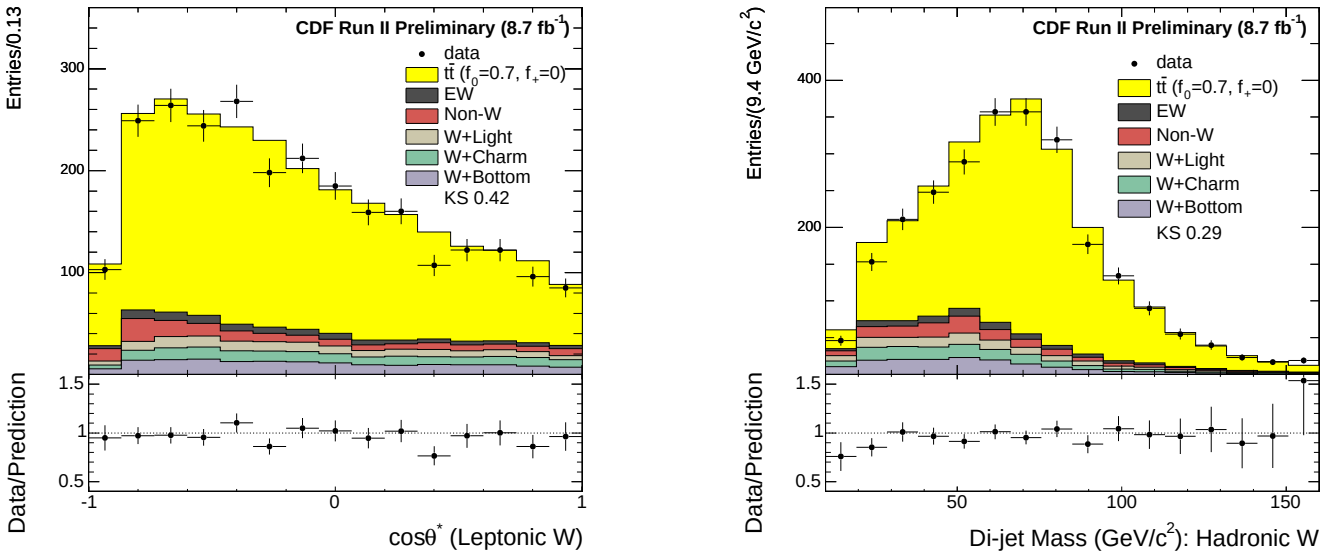

FIG. 1: Comparison of two kinematic variables for data and simulation for W polarization fractions at the SM predicted values. Plotted are the $\cos\theta^*$ of the leptonically decaying W boson (left) and the invariant mass of the pair of light quark jets from the hadronically (right), for the reconstruction chosen as most likely by the per-event likelihood.

VI. CALIBRATION AND VALIDATION

We calibrate the results of the likelihood fit using the simulated $t\bar{t}$ and background samples, and the sample composition of Table I. For the simultaneous measurement of f_0 and f_+, we find our estimate $f_{0,\mathrm{m}}$ is related to the true value of f_0 by $f_{0,\mathrm{m}} = (0.87 \pm 0.01) f_0 + (-0.14 \pm 0.01)$ and our estimate of $f_{+,\mathrm{m}}$ is related to the true value of f_+ and f_0 by $f_{+,\mathrm{m}} = (1.23 \pm 0.01) f_+ + (0.16 \pm 0.02) f_0 + (0.10 \pm 0.01)$. We use these calibration functions and the measured polarization fractions to extract the true polarization fractions. For our measurement of f_0 with $f_+ = 0$, we find our estimate $f_{0,\mathrm{m}} = (1.12 \pm 0.02) f_0 + (-0.11 \pm 0.02)$, and for our measurement of f_+ with $f_0 = 0.7$, we find our estimate $f_{+,\mathrm{m}} = (1.10 \pm 0.03) f_+ + (0.04 \pm 0.01)$. The uncertainties on the coefficients of the calibration functions are included in the method-related systematic uncertainties, which cover possible biases due to the calibration procedure. The differences between our measured values and the true values arise because the signal and background probabilities used in the likelihood do not accurately model the effects of extra jets arising from initial and final state radiation

(ISR/FSR) nor the full set of contributing background processes. Even though the likelihood can be calculated only for the physical values of f_0 and f_+, after calibration the corrected measured values can be slightly outside their physical ranges.

The robustness of the fitting procedure over all physical values of (f_0,f_+) has been tested with simulated experiments, using the number of observed data events and the sample composition of Table I. In all cases, the method is unbiased. Near the physical boundaries, we find that the statistical uncertainty is underestimated by as much as a factor of 1.5. We apply a correction to the statistical uncertainty in these regions. Assuming the SM, the expected statistical uncertainties after all corrections for the simultaneous measurement are ± 0.075 and ± 0.047 for f_0 and f_+, respectively.

VII. SYSTEMATIC UNCERTAINTIES

Various sources of systematic uncertainty affecting the measurement are summarized in Table II. All systematic uncertainties are determined by performing simulated experiments in which the systematic parameter in question is varied, the default method and calibrations are applied, and the shifts in the mean measured polarization fractions are used to quantify the uncertainty. The leading sources of systematic uncertainty arise from MC modeling of initial and final state radiation (ISR/FSR), choice of PDFs, choice of MC generator, uncertainties on the measured jet energy, and the background shape and normalization. The method-related uncertainty includes propagating the uncertainty on the fit parameters of the calibration functions, including their correlations. Systematic uncertainties due to multiple hadron interactions (MHI) and color reconnection (CR) were not assigned in the previous version of the analysis, [7]. The MHI uncertainty, which takes into account of the increasing instantaneous luminosity in this dataset that is not modeled properly in the MC, had a negligible effect in [7]. The CR systematic uncertainty [28] is evaluated using MC samples generated with and without CR effects adopting different tunes [29] of PYTHIA. The MC generator uncertainty is evaluated by comparing between $t\bar{t}$ MC generated by Pythia and MC@NLO [27] with parton showering done by Herwig; it includes uncertainties from not using the NLO matrix element in the generator, choice of parton shower model and modeling of $t\bar{t}$ spin-correlation. In [7] we only listed uncertainty from choice of parton shower model. All shifts are evaluated at the SM helicity fraction.

TABLE II: Summary of systematic uncertainties.

Source	Δf_0	Δf_+	Δf_0 simultaneous	Δf_+ simultaneous
ISR/FSR	0.011	0.017	0.022	0.023
JES	0.016	0.017	0.010	0.022
PDF	0.024	0.013	0.009	0.016
Background	0.007	0.011	0.049	0.036
Method-related	0.014	0.020	0.018	0.016
MC generator	0.012	0.009	0.023	0.011
Color reconnection	0.013	0.010	0.020	0.016
MI	0.009	0.013	0.008	0.014
Total	0.040	0.040	0.067	0.058

VIII. RESULTS

With 2574 events in data we perform the measurements with three different scenarios of top-quark decay. For the simultaneous measurement of f_0 and f_+, after all corrections, we measure

$$\begin{aligned} f_0 &= 0.726 \pm 0.066(\text{stat}) \pm 0.067(\text{syst}) \\ f_+ &= -0.045 \pm 0.043(\text{stat}) \pm 0.058(\text{syst}). \end{aligned}$$

The statistical correlation between f_0 and f_+ is $\rho = -0.51$. We estimate a shift of $\mp(0.010 \pm 0.004)$ in f_0 and $\pm(0.012 \pm 0.002)$ in f_+ per ± 1 GeV/c^2 shift in the top quark mass from the central value of 172.5 GeV/c^2. Figure 2 shows the data-fit result and the coverage in the 2-dimension in the (f_0, f_+) plane at 68.27% confidence level (CL), obtained from the contours with $-\ln(L/L_{\max}) = 0.5$ and 1.15 in data, respectively. Here $L_{\max}$ is the maximum value for the likelihood L.

Fixing $f_+ = 0$ we measure after all corrections $f_0 = 0.683 \pm 0.042(\text{stat}) \pm 0.040(\text{syst})$. Fixing $f_0 = 0.70$, we measure after all corrections $f_+ = -0.025 \pm 0.024(\text{stat}) \pm 0.040(\text{syst})$. We estimate a shift of $\pm(0.007 \pm 0.002)$ in f_0 and $\pm(0.008 \pm 0.001)$ in f_+ per ± 1 GeV/c^2 shift in the top-quark mass from the central value of 172.5 GeV/c^2.

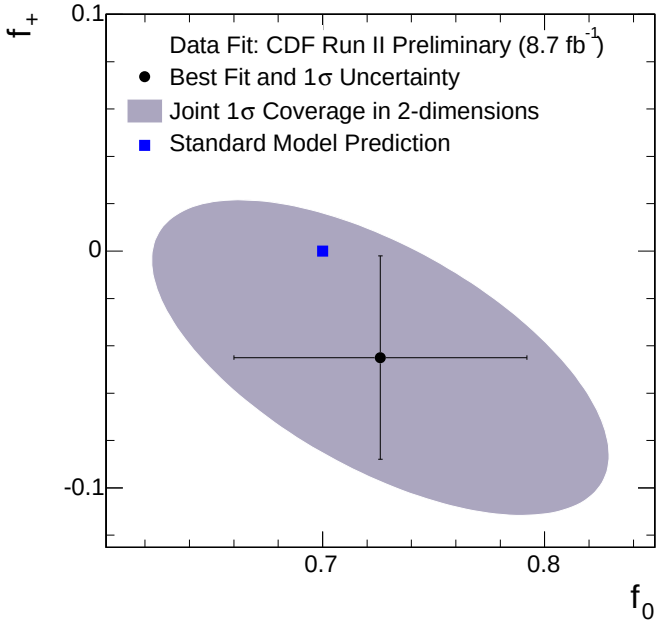

FIG. 2: Data-fit results for simultaneous measurement of f_0 and f_+ using events in 8.7 fb^{-1} data sample. The dot with uncertainty shows the point of maximum likelihood and 1-σ uncertainty obtained based on the $-\ln(L/L_{\max}) = 0.5$ contour. The shaded ellipse corresponds to a 68.27% coverage in 2-dimension in the (f_0, f_+) plane. The square marker shows the SM prediction.

IX. CONCLUSION

In summary, we have measured the polarization of the W boson in top-quark decays using a matrix-element method in 8.7 fb^{-1} of CDF II data. This result improves the statistical precision on both the model-independent and model-dependent determinations of the f_0 and f_+ by a factor of 1.6 compared to the previous CDF measurement [7] in the lepton+jets channel. The results have compatible precisions compared to [6] and a similar level of systematic precisions compared to [10]. Our results are consistent with the SM.

Acknowledgments

We thank the Fermilab staff and the technical staffs of the participating institutions for their vital contributions. This work was supported by the U.S. Department of Energy and National Science Foundation; the Italian Istituto Nazionale di Fisica Nucleare; the Ministry of Education, Culture, Sports, Science and Technology of Japan; the Natural Sciences and Engineering Research Council of Canada; the National Science Council of the Republic of China; the Swiss National Science Foundation; the A.P. Sloan Foundation; the Bundesministerium fuer Bildung und Forschung, Germany; the Korean Science and Engineering Foundation and the Korean Research Foundation; the Particle Physics and Astronomy Research Council and the Royal Society, UK; the Russian Foundation for Basic Research; the Comision Interministerial de Ciencia y Tecnologia, Spain; and in part by the European Community's Human Potential Programme under contract HPRN-CT-20002, Probe for New Physics.

---

[1] Charge-conjugate modes are included implicitly throughout this paper.
[2] K. Nakamura *et al* (Particle Data Group),J. Phys. G **37**, 075021 (2010) and 2011 partial update for the 2012 edition.
[3] J. Aguilar-Saavedra *et al.*, Eur. Phys. J. C **50**, 519 (2007).
[4] T. Aaltonen *et al.* (CDF Collaboration), Phys. Rev. Lett. **99**, 151801 (2007).
[5] M. Fischer *et al.*, Phys. Rev. D **63**, 031501(R) (2001); H. S. Do *et al.*, Phys. Rev. D **67**, 091501(R) (2003).
[6] T. Aaltonen *et al.* (CDF and D0 Collaborations), Phys. Rev. D **85**, 071106(R) (2012).
[7] T. Aaltonen *et al.* (CDF Collaboration), Phys. Rev. Lett. **105**, 042002 (2010).
[8] T. Aaltonen *et al.* (CDF Collaboration), Submitted for publication (arXiv:1205.0354v1 [hep-ex]).
[9] V. M. Abazov *et al.* (D0 Collaboration), Phys. Rev. D **83** 032009 (2011).
[10] G. Aad *et al.* (ATLAS Collaborations), Submitted for publication (arXiv:1205.2484v1 [hep-ex]).
[11] D. Acosta *et al.* (CDF Collaboration), Phys. Rev. D **71**, 031101(R) (2005).
[12] We use a cylindrical coordinate system where the z axis is along the proton beam direction and θ is the polar angle. Pseudorapidity is $\eta = -\ln\tan(\theta/2)$, while transverse momentum is $p_T = |p|\sin\theta$, and transverse energy is $E_T = E\sin\theta$. Missing transverse energy, $\not\!\!E_T$, is defined as the magnitude of $-\sum_i E_T^i \hat{n}_i$, where $\hat{n}_i$ is the unit vector in the azimuthal plane that points from the beam line to the i^{th} calorimeter tower.
[13] A. Abulencia *et al.* (CDF Collaboration), Phys. Rev. D **74**, 072006 (2006); T. Aaltonen *et al.* (CDF Collaboration), Phys. Rev. Lett. **100**, 211801 (2008).
[14] V. M. Abazov *et al.* (D0 Collaboration), Nature **429**, 02589 (2004); V. M. Abazov *et al.* (D0 Collaboration), Phys. Lett. B**617**, 1 (2005).
[15] T. Aaltonen *et al.* (CDF Collaboration), Phys. Lett. B**674**, 160 (2009).
[16] A. Abulencia *et al.* (CDF Collaboration), Phys. Rev. Lett. **98**, 072001 (2007); A. Abulencia *et al.* (CDF Collaboration), Phys. Rev. D **75**, 052001 (2007); A. Abulencia *et al.* (CDF Collaboration), Phys. Rev. D **73**, 111103 (2006); D. Acosta *et al.* (CDF Collaboration), Phys. Rev. D **71**, 031101 (2005).
[17] A. Abulencia *et al.* (CDF Collaboration), Phys. Rev. Lett. **99**, 182002 (2007).
[18] G. Mahlon and S. Parke, Phys. Lett. B**411**, 173 (1997); G. Mahlon and S. Parke, Phys. Rev. D **53**, 4886 (1996).
[19] F. A. Berends, W. T. Giele, and H. Kuijf, Nucl. Phys. B**321**, 39 (1989).
[20] A. Bhatti *et al.*, Nucl. Instrum. Methods A **566**, 2 (2006).
[21] D. Acosta *et al.* (CDF Collaboration), Phys. Rev. D **71**, 052003 (2005).
[22] D. Acosta *et al.* (CDF Collaboration), Phys. Rev. Lett. **97**, 082004 (2006), T. Aaltonen *et al.* (CDF Collaboration), Phys. Rev. Lett. **105**,012001 (2010).
[23] G. Corcella *et al.*, J. High Energy Phys. **01**, 10 (2001).
[24] T. Sjostrand *et al.*, Comput. Phys. Commun. **135**, 238 (2001).
[25] M. Mangano *et al.*, J. High Energy Phys. **07**, 001 (2003).
[26] J. Alwall *et al.*, J. High Energy Phys. **09**, 28 (2007).
[27] S. Frixione and B. R. Webber, J. High Energy Phys. **06** 029 (2002).
[28] D. Wicke and P. Z. Skands, Eur. Phys. J. C **52**, 133 (2007).
[29] T. Aaltonen *et al.* (CDF Collaboration), Phys. Rev. D **81**, 031102(R) (2010).

APPENDIX A: ADDITIONAL PLOTS

1. Plots : Calibration, Sensitivity and Results of the Simultaneous Measurement

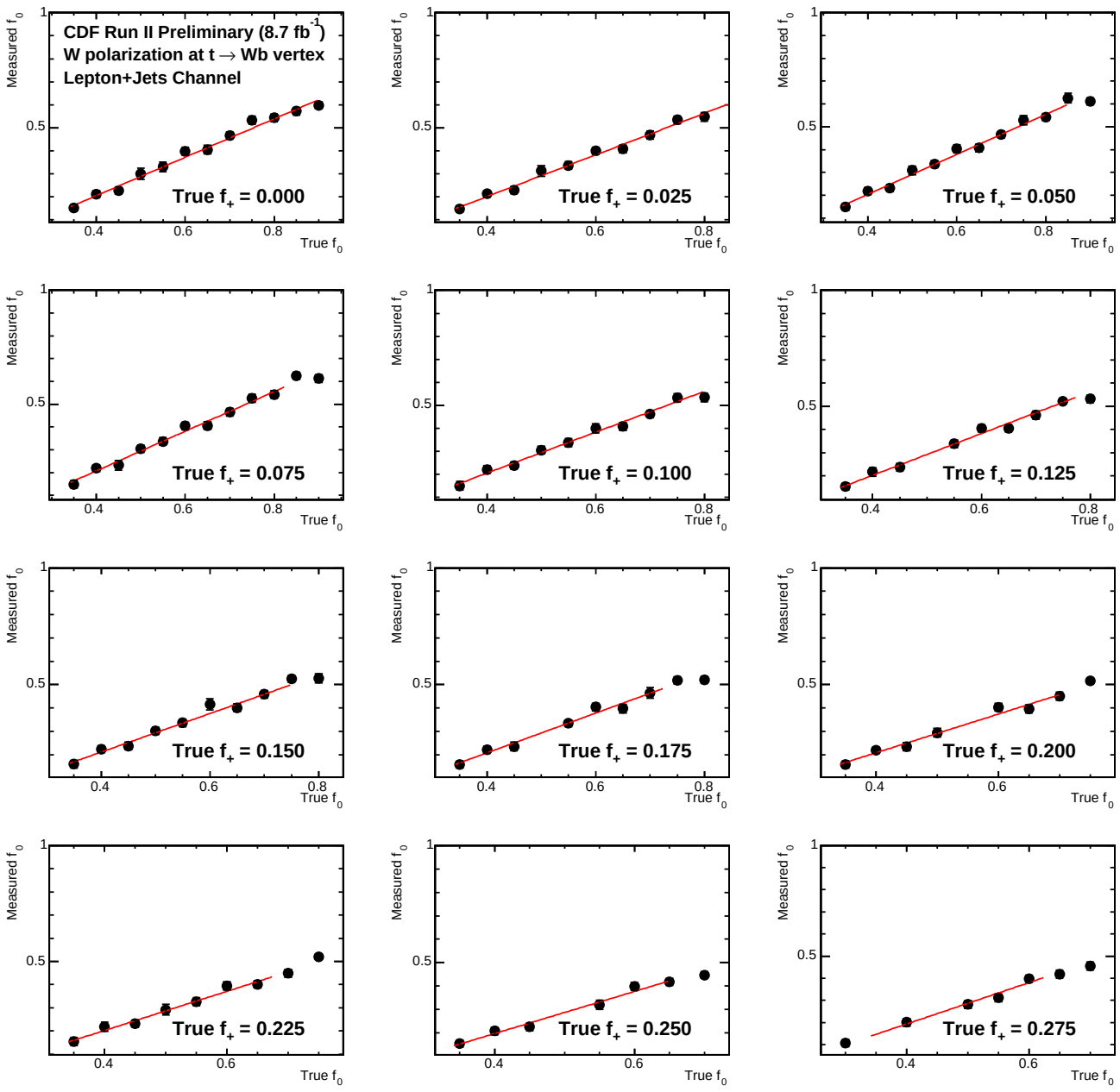

FIG. 3: The f_0 calibration curves from the simultaneous fit in slices of f_+. In each plot the measured f_0 determined from the 2-dimension likelihood curve is plotted versus the MC input f_0 value. A first order polynomial fit is also shown and will be used to derive the correction functions for the simultaneous fits. Each point on this calibration curve uses one large high statistics simulated experiment constructed using the relative fractions of signal and background contributions given in Table I .

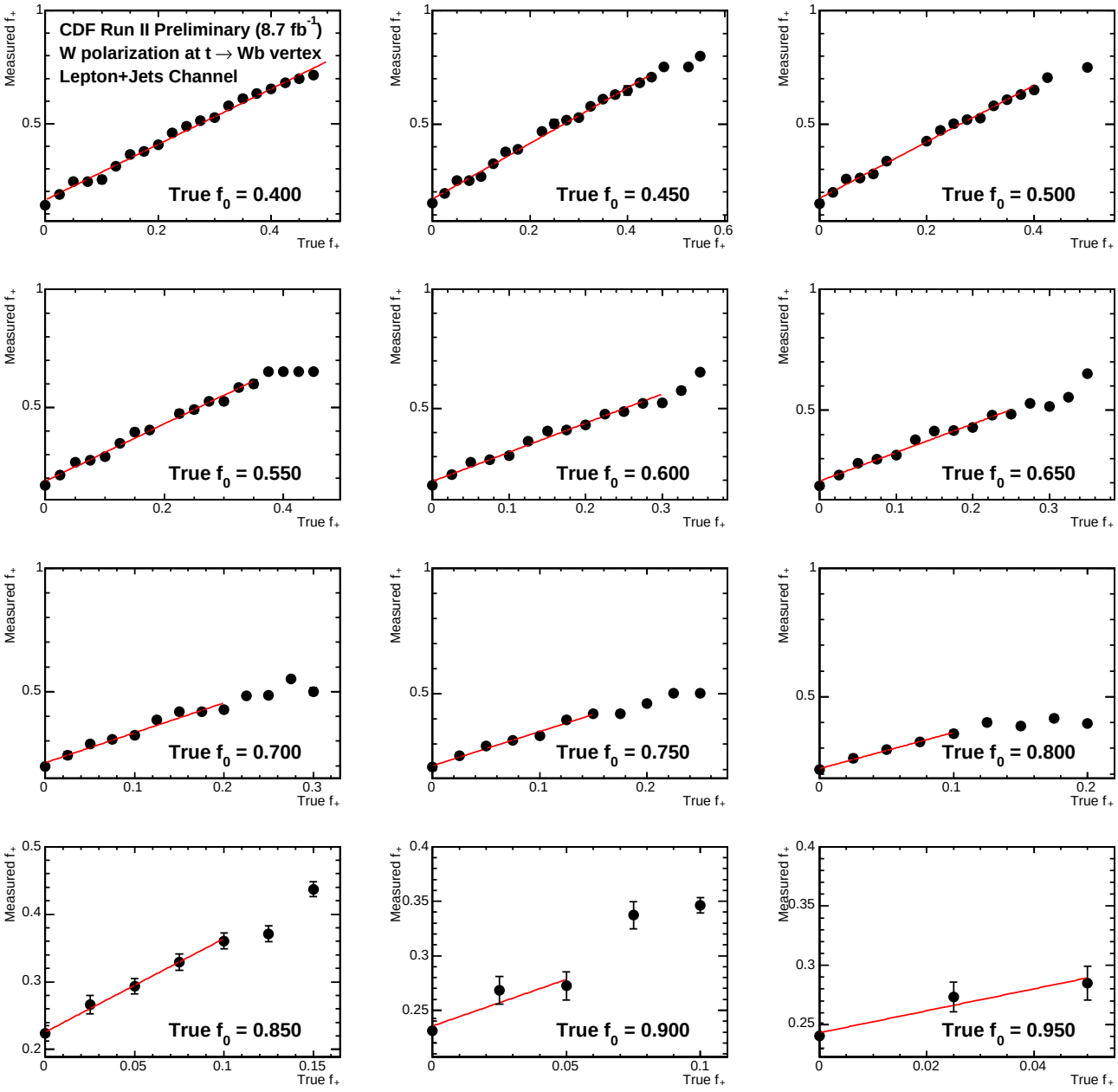

FIG. 4: The f_+ calibration curves from the simultaneous fit in slices of f_0. In each plot the measured f_+ determined from the 2-dimension likelihood curve is plotted versus the MC input f_+ value. A first order polynomial fit is also shown and will be used to derive the correction functions for the simultaneous fits. Each point on this calibration curve uses one large high statistics simulated experiment constructed using the relative fractions of signal and background contributions given in Table I.

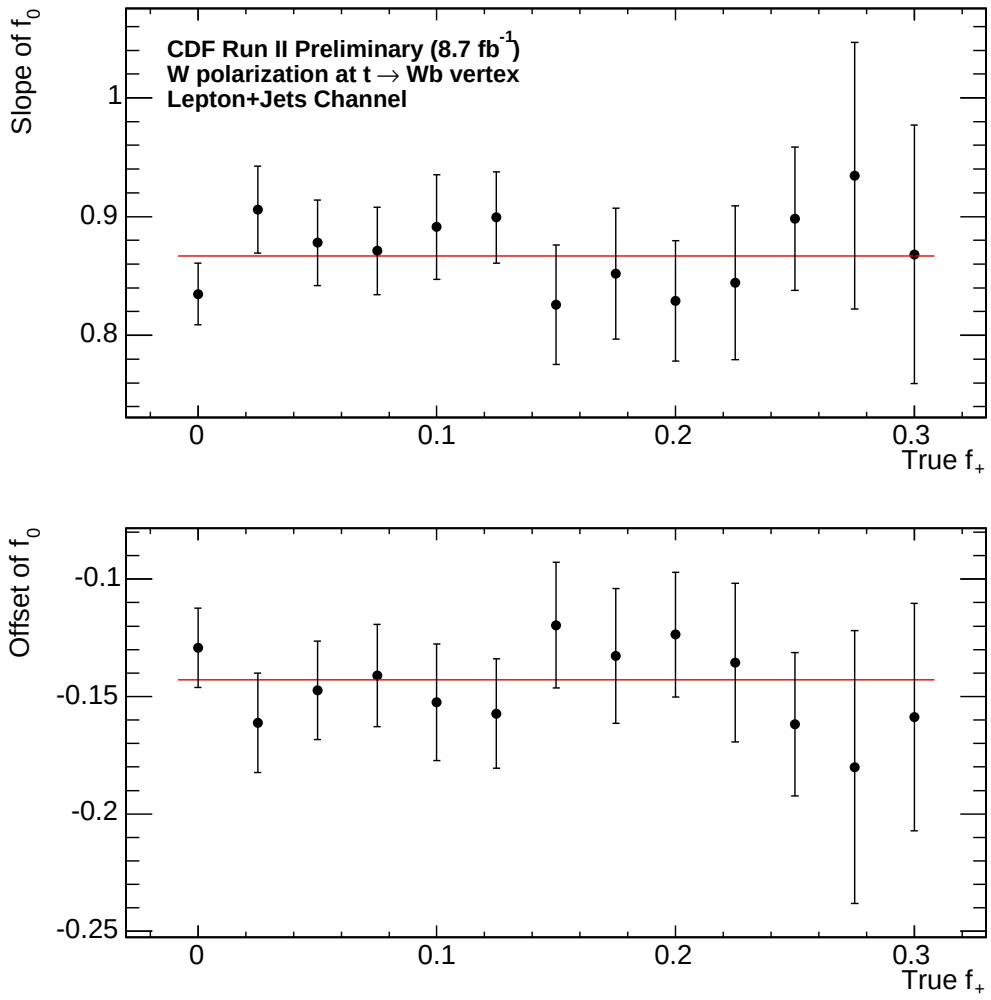

FIG. 5: The fitted slope (top) and offset (bottom) from the f_0 calibration curves as a function of input f_+ values. Neither the slope nor the offset vary significantly as a function of f_+. We use these curves to derive the final simultaneous calibration functions discussed in the text.

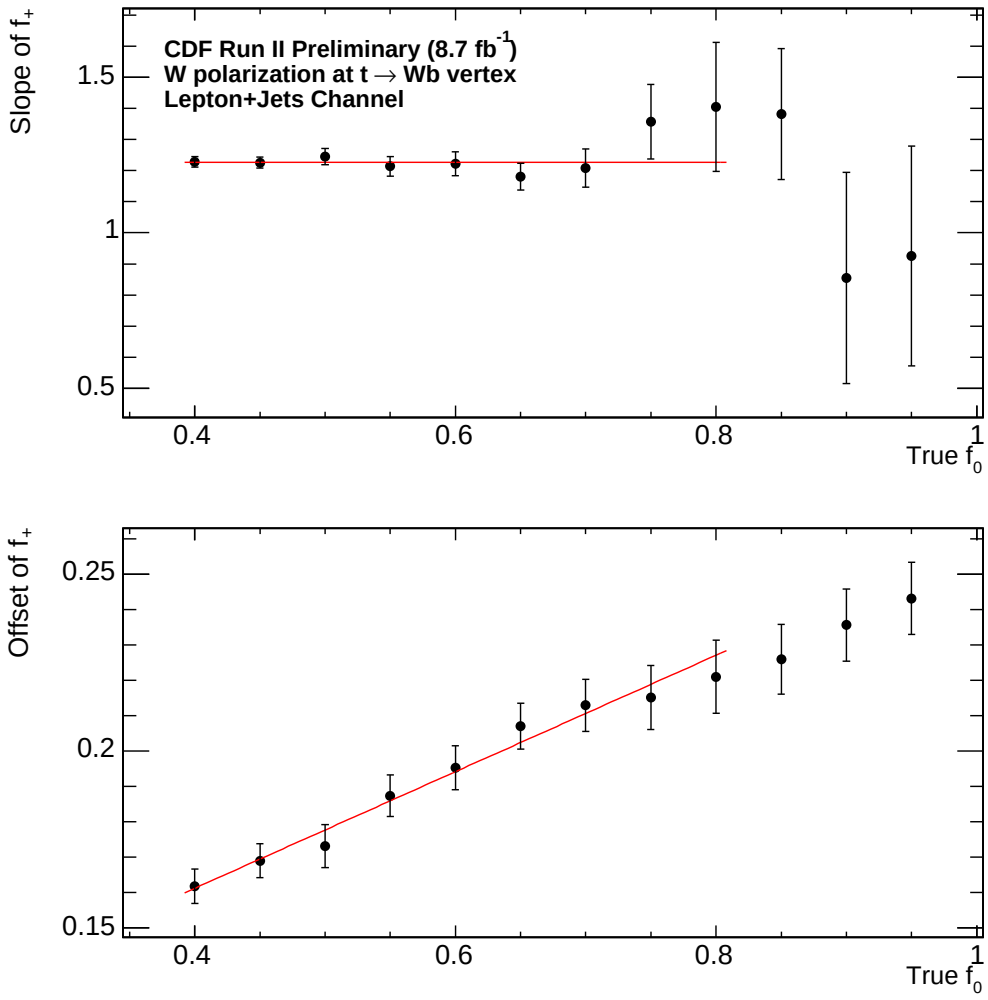

FIG. 6: The fitted slope (top) and offset (bottom) from the f_+ calibration curves as a function of input f_0 values. While the slope does not vary significantly as a function of f_0, the offset does. We include this effect in the final simultaneous calibration functions discussed in the text.

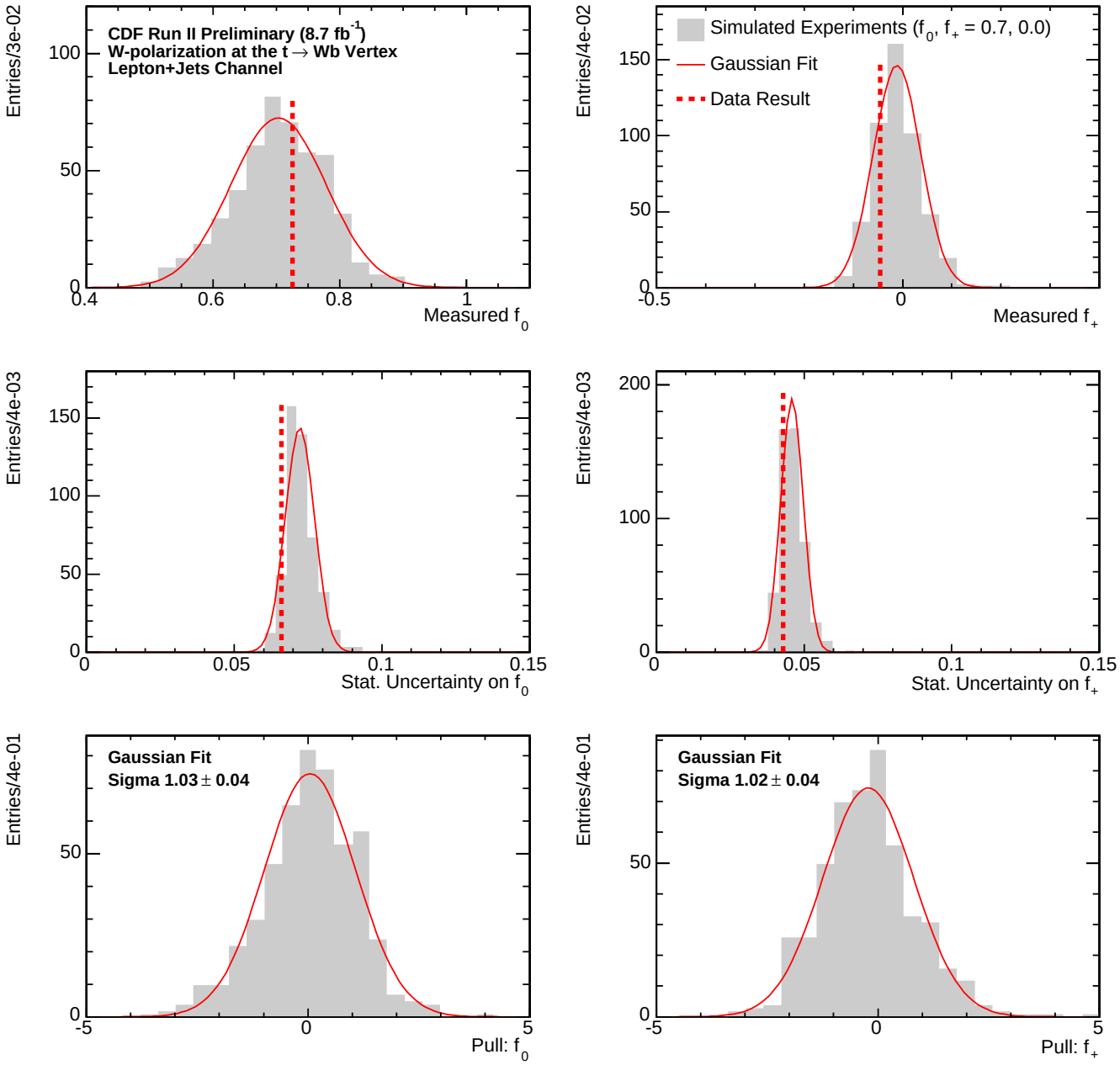

FIG. 7: Distributions of the corrected polarization fractions (top) and their statistical uncertainty (middle) determined from 8.7 fb^{-1} sized simulated experiments constructed assuming the SM $t\bar{t}$ polarization fractions. The dashed lines indicate the quantities observed from the fits to the CDF data. The corresponding pull distribution is also shown (bottom). These plots correspond to the simultaneous fit results. The f_0 results are on the left, the f_+ are on the right.

2. Plots : Calibration, Sensitivity and Results of the Model-Dependent Measurement

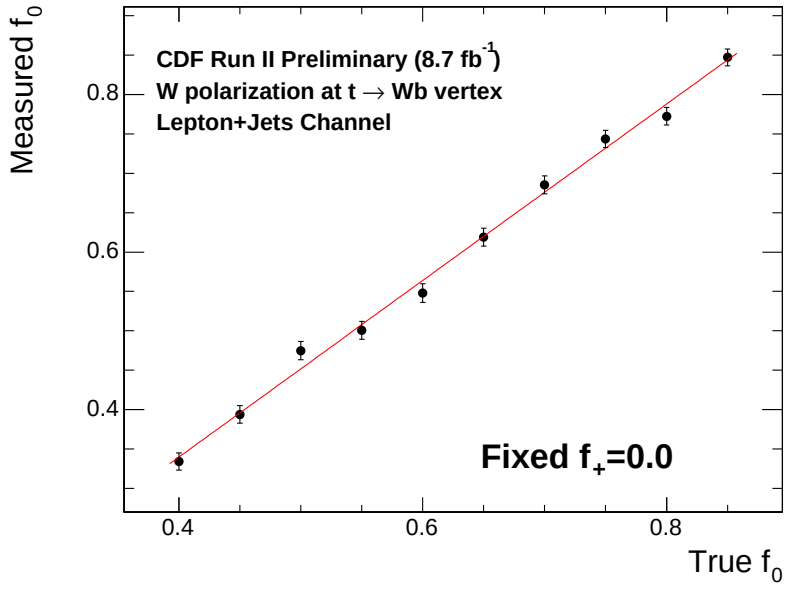

FIG. 8: Calibration curve for the model-dependent fits to determine f_0. The measured f_0 determined from the likelihood curve is plotted versus the MC input f_0 value. A first order polynomial fit is shown and is used to corrected the measured f_0 to the true value. Each point on this calibration curve uses one large high statistics simulated experiment constructed using the relative fractions of signal and background contributions given in Table I.

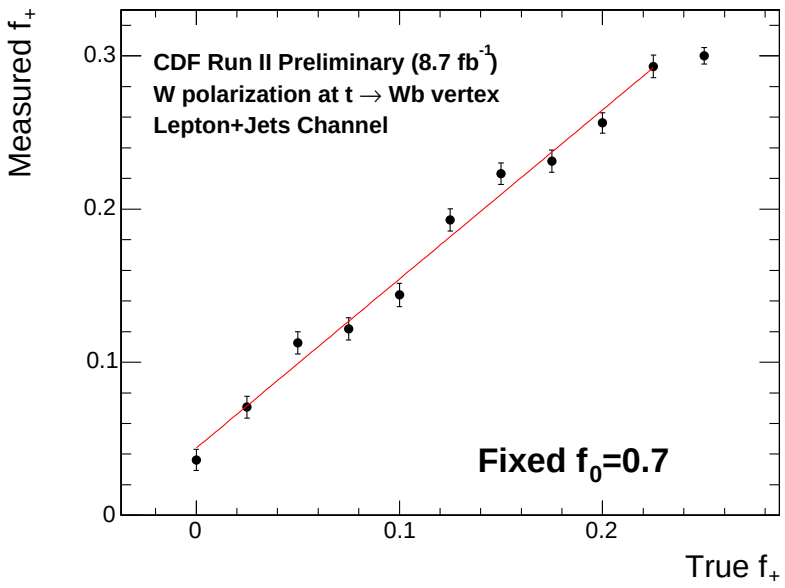

FIG. 9: Calibration curve for the model-dependent fits to determine f_+ using the modified likelihood. The measured f_+ determined from the likelihood curve is plotted versus the MC input f_+ value. A first order polynomial fit is shown and is used to correct the measured f_+ to the true value. Each point on this calibration curve uses one large high statistics simulated experiment constructed using the relative fractions of signal and background contributions given in Table I.

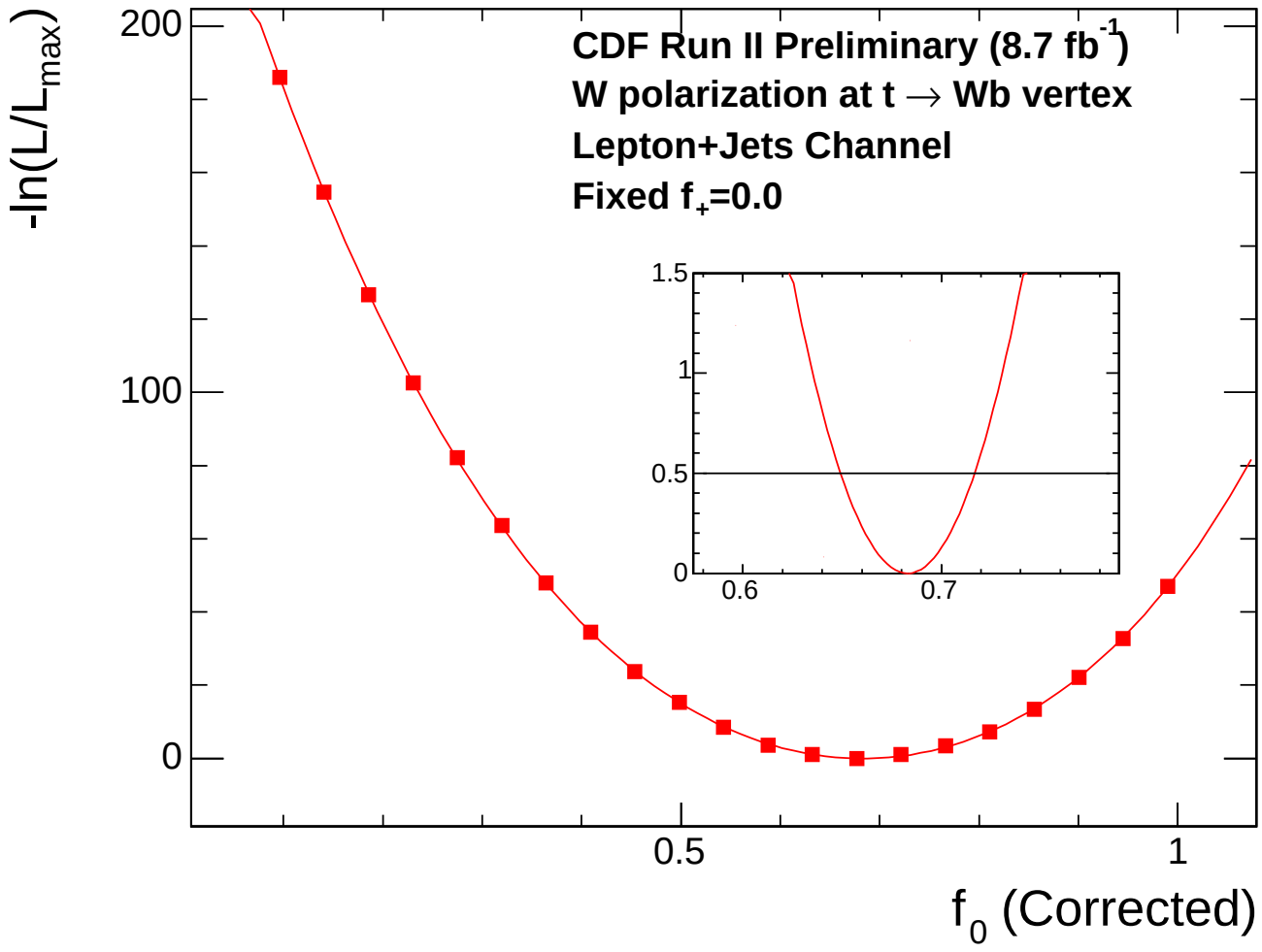

FIG. 10: The negative-log-likelihood curves from a fit to the 2574 data events for the model-dependent determination of f_0.

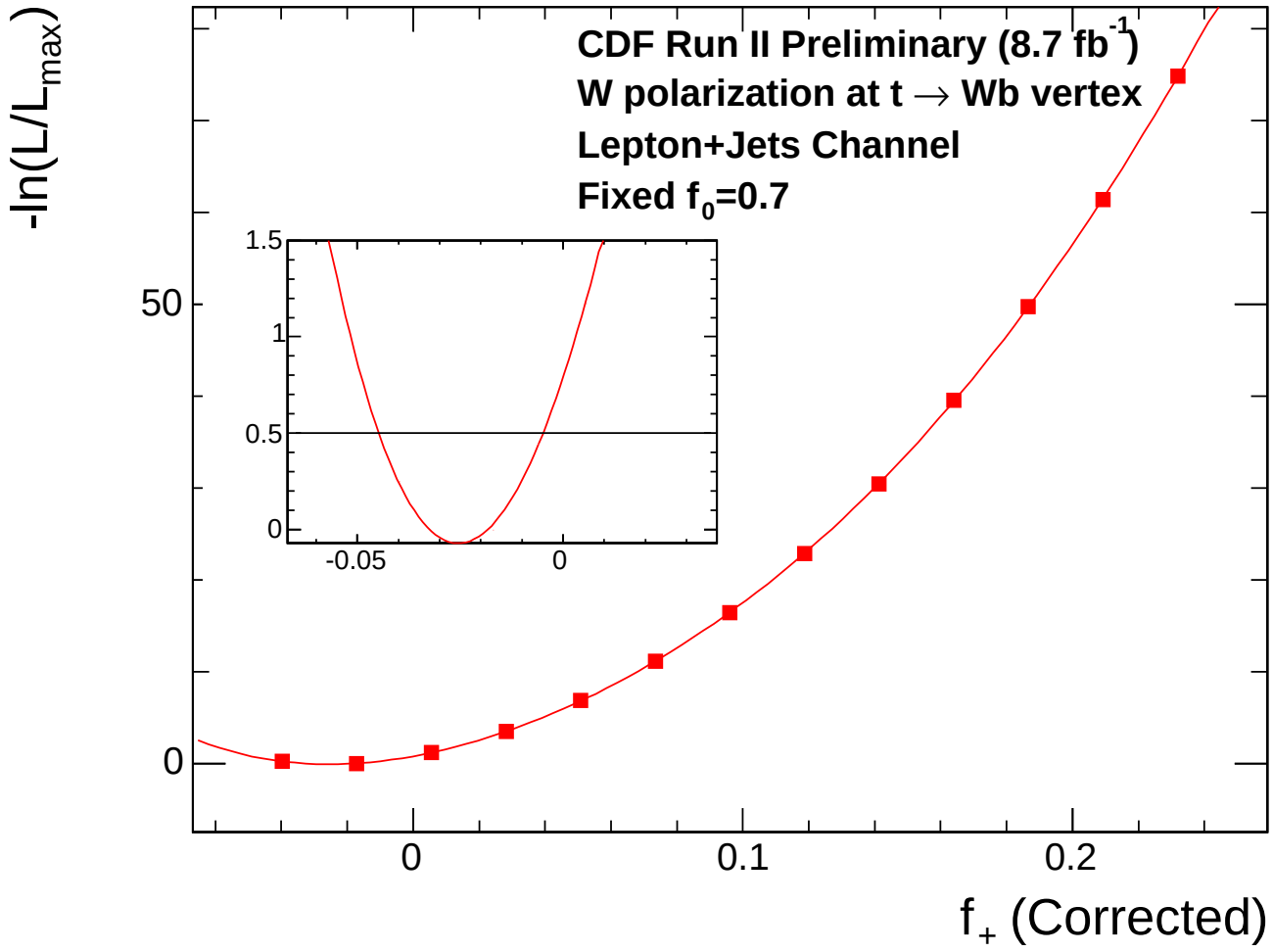

FIG. 11: The negative-log-likelihood curves from a fit to the 2574 data events for the model-dependent determination of f_+.

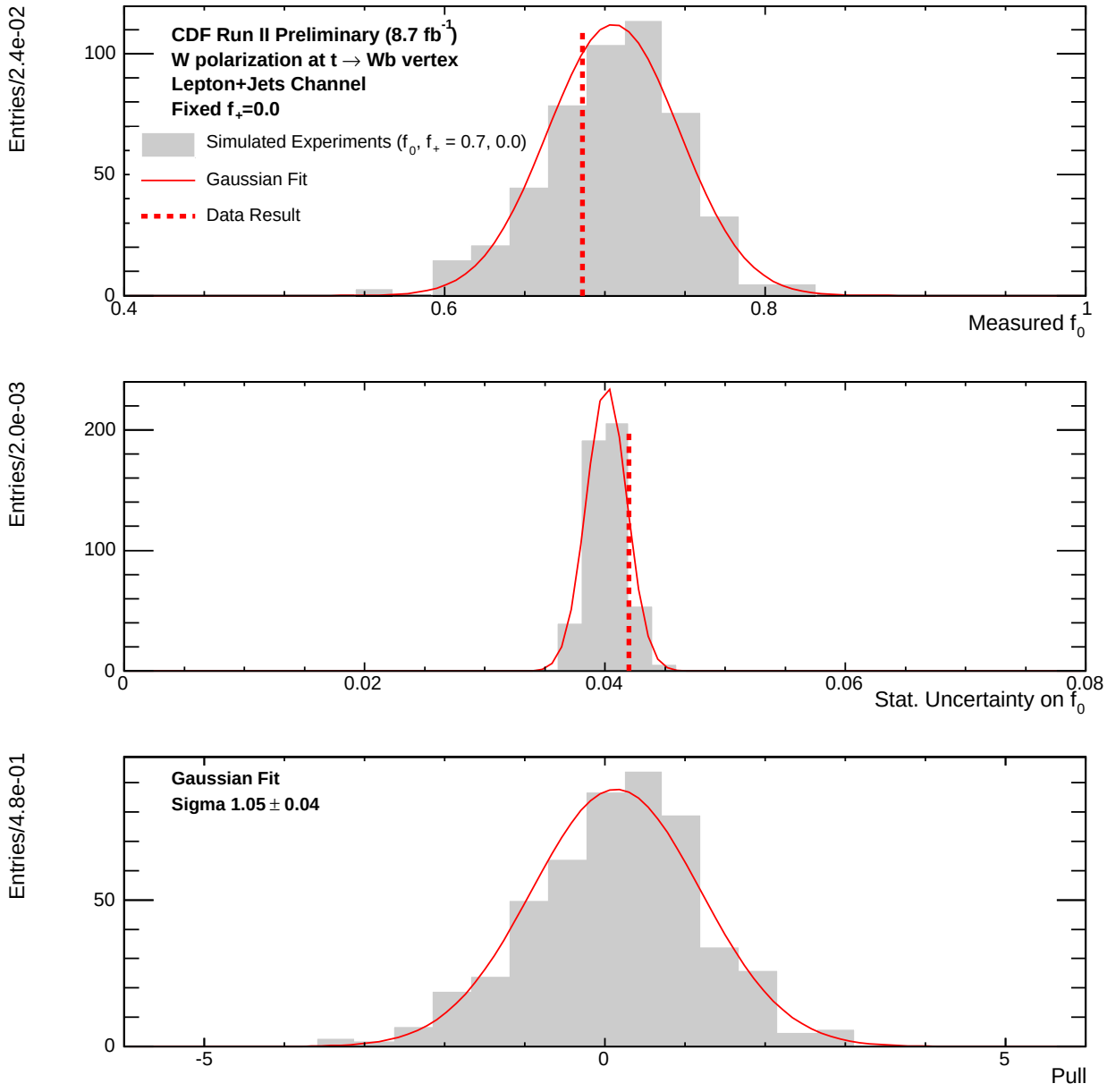

FIG. 12: Distributions of the corrected polarization fraction (top) and its statistical uncertainty (middle) determined from 8.7 fb^{-1} sized simulated experiment constructed assuming the SM $t\bar{t}$ polarization fractions. The dashed lines indicate the quantities observed from the fits to the CDF data. The pull distribution is also shown (bottom). These correspond to model-dependent fits determining f_0.

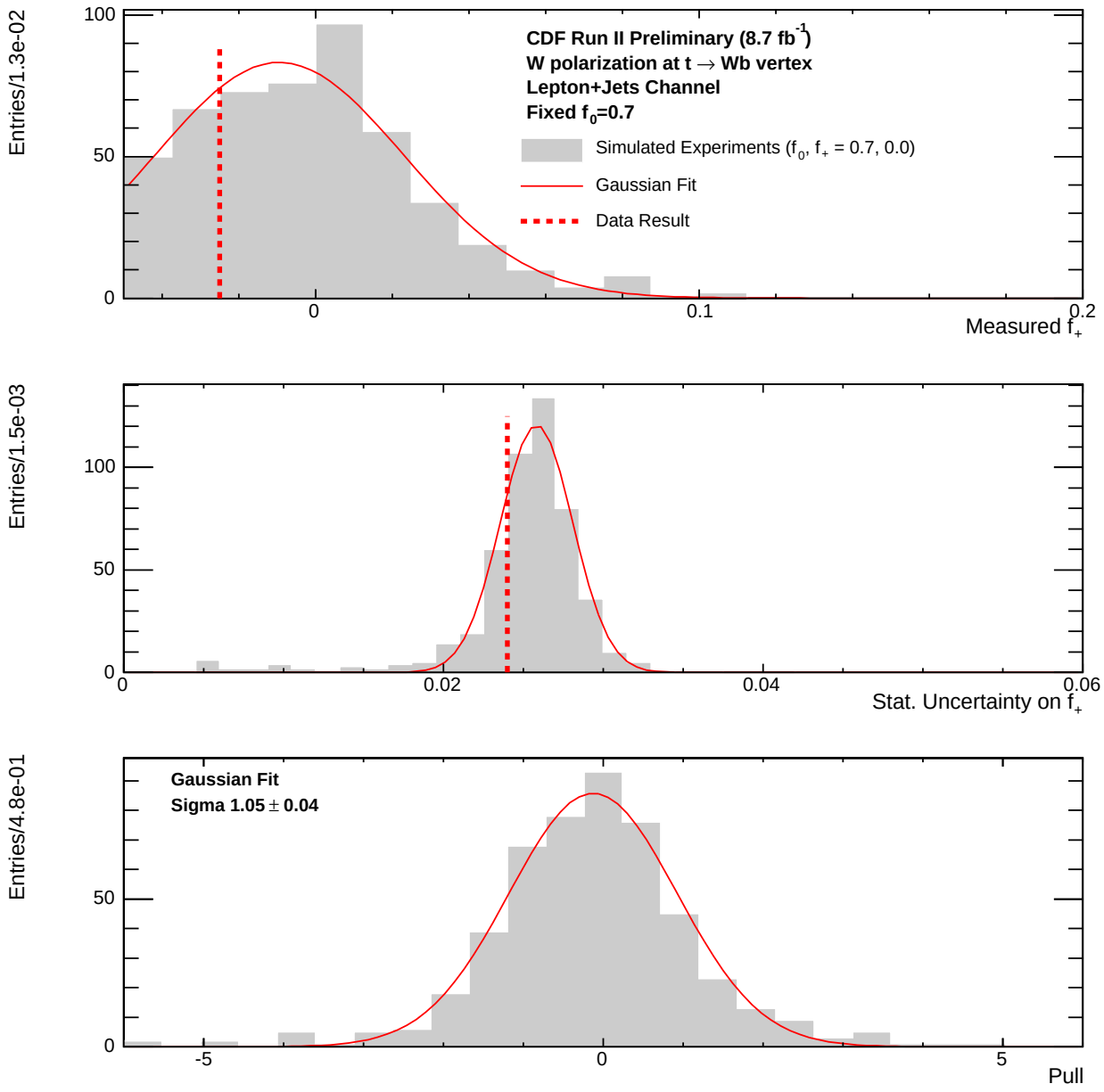

FIG. 13: Distributions of the corrected polarization fraction (top) and its statistical uncertainty (middle) determined from 8.7 fb^{-1} sized simulated experiment constructed assuming the SM $t\bar{t}$ polarization fractions. The dashed lines indicate the quantities observed from the fits to the CDF data. The pull distribution is also shown (bottom). These correspond to model-dependent fits determining f_+.